https://doi.org/10.5194/egusphere-2025-5457
Preprint. Discussion started: 2 January 2026

Physically Segmented Plasma Parameterization of Titan's Ionosphere for Nonlinear Wave Dynamics

Hamid Reza Pakzad *
Department of Physics, Bojnourd Branch, Islamic Azad University, Bojnourd, Iran
Kurosh Javidan †
Department of Physics, Faculty of Science, Ferdowsi University of Mashhad, 9177948974 Mashhad, Iran

Abstract

We present a physically segmented plasma-parameter framework for Titan's ionosphere, derived from in-situ Cassini measurements and optimized for nonlinear wave–dynamics studies. The models provide altitude-dependent ion temperature, electron temperature, and electron density profiles that combine physical interpretability with computational readiness.

Ion temperature is described by three regimes: isothermal lower layer, exponential-heating middle layer, and magnetospheric power-law tail. Achieving segment-wise $R^2 > 0.98$ with transition altitudes ($h_1 \approx 1000$ km, $h_2 \approx 1800$ km) consistent with prior observations. Electron temperature is modeled by a Gaussian rise in the lower ionosphere and a double-Gaussian plus baseline in the upper ionosphere, capturing both broad and localized heating features. Electron density is represented by a four-segment profile resolving production, recombination, plateau, and magnetospheric decay regimes, outperforming smooth empirical models with $R^2 \approx 0.997$.

These parameterizations are accurate, physically grounded, and numerically efficient, enabling realistic simulations of ion–acoustic solitons, nonlinear wave propagation, and energy transport in Titan's ionosphere. The framework is adaptable to other weakly magnetized planetary bodies and can be extended to include solar-cycle, latitude, and magnetospheric coupling effects.

Keywords: Titan's ionosphere; plasma parameterization; nonlinear wave propagation; ion–acoustic solitons; Cassini observations

1 Introduction

Titan's ionosphere is among the most chemically rich and dynamic plasma environments in the solar system, providing a natural laboratory for studying extraterrestrial plasma processes. This partially ionized layer of Titan's upper atmosphere extends from roughly 800 km to beyond 3000 km in altitude and consists primarily of electrons, positive ions such as CH_5^+, $C_2H_5^+$, and H_3^+, as well as heavy negative ions, many of which are complex organic molecules. On the dayside, direct solar illumination—especially extreme ultraviolet (EUV) radiation—produces markedly higher ionospheric densities (T et al., 2009).

The dominant ionization source below ∼1200 km is solar UV and EUV radiation. Additional ionization arises from photoelectrons and energetic electrons precipitating from Saturn's magnetosphere, while galactic cosmic rays become increasingly important below ∼900 km. A pronounced electron density peak occurs near 1200 km, reaching ∼5000 cm^{-3}. Below this peak (≈950–1100 km), production and recombination processes dominate, whereas above it (1200–2400 km) the ionosphere transitions into a diffusion-dominated regime with declining ion production. Beyond 2400 km, densities decrease more gradually, following a power-law profile shaped by magnetospheric inputs and weak recombination (Galand et al., 2010).

*Email: ttaranomm83@yahoo.com
†Email:javidan@um.ac.ir

https://doi.org/10.5194/egusphere-2025-5457
Preprint. Discussion started: 2 January 2026

Like Earth's ionosphere, Titan's plasma environment responds dynamically to solar conditions. Electron density varies with solar zenith angle (SZA) and solar activity, increasing during solar maximum. On the dayside, EUV flux strongly controls ionization, while the nightside maintains plasma primarily through magnetospheric transport (Agren et al., 2009).

One of the Cassini mission's most surprising discoveries was the detection of heavy negative ions, some exceeding several thousand atomic mass units, in the 900–1200 km region. These species, thought to be complex organic anions or tholin precursors, form through electron attachment to hydrocarbons and nitriles in regions where dense neutrals coexist with low-energy electrons. Negative ions influence ion-acoustic wave propagation, dispersion, and phase velocity in the lower ionosphere but become negligible above ∼1500 km (Edberg et al., 2013).

At altitudes above ∼2400 km, Saturn's magnetosphere dominates, with plasma transport, wave–particle interactions, and induced magnetic fields controlling energy transfer. Here, the electron density follows a power-law decay rather than the exponential decline characteristic of lower layers (Westlake et al., 2011).

Negative ions in Titan's ionosphere represent one of the most surprising discoveries made by the *Cassini* mission. These ions were detected by the CAPS-ELS (Electron Spectrometer) during flybys starting in 2005. The first evidence was reported by Coates et al. (Coates et al., 2007), revealing negative ions with masses up to several thousand atomic mass units (amu). Many of these are thought to be complex organic anions or tholin precursors, formed through electron attachment to neutral hydrocarbons and nitriles in the 900–1200 km region where dense neutrals and low-energy electrons coexist (Desai et al., 2017).

While Cassini's Radio and Plasma Wave Science (RPWS) instrument detected solitary wave structures near Titan (particularly at 1000–1400 km), most theoretical models assume constant ionospheric parameters, neglecting their strong altitude dependence. Early work by Ahmed et al (S et al., 2022, 2020). modeled small-amplitude ion–acoustic solitary waves on Titan's dayside and nightside using fixed plasma parameters, enabling analytical solutions but sacrificing vertical resolution. More recent studies incorporating non-Maxwellian particle distributions have shown improved agreement with observed wave structures, highlighting the need for realistic plasma profiles.

Recent efforts to incorporate non-Maxwellian distributions in Titan's plasma models suggest that such approaches yield more accurate representations of solitary structures (Yahia et al., 2021). These findings support the idea that kinetic features and realistic plasma distributions are important when modeling wave phenomena in planetary ionospheres.

To address the limitations of existing studies, the present work introduces altitude-dependent plasma parameters based on Cassini observations. By capturing the real vertical structure of Titan's ionosphere, this study aims to develop a more accurate, altitude-resolved model of ion-acoustic solitary waves. More broadly, the framework may be extended to other weakly magnetized planetary bodies in the solar system.

2 Ion Temperature in Titan's Upper Atmosphere

The observed ion temperature profile on Titan's nightside reveals three distinct altitude regimes, each dominated by different physical processes. Between approximately 960 and 1200 km, the temperature shows fluctuations and dips to a local minimum (at ∼900 km ion temperature is about ∼149±3 K (V et al., 2006)). Above 1200 km, it rises steadily, reaching lower than 175 K near 1600 km (Richard et al., 2011). The transition zone between about 1000 and 1200 km marks a shift from a lower ionospheric layer dominated by collisional cooling and radiative losses to an upper region where external heating processes prevail. Possible high-altitude heating sources include energy deposition by suprathermal electrons, magnetospheric particle precipitation from Saturn's environment, wave–particle interactions, turbulence, and ambipolar electric fields that drive upward ion flows and heating.

Ion temperature data for altitudes below 1000 km are taken from (V et al., 2006), those between 1000 and 2400 km from (**?**), and data above 1850 km from (T et al., 2009; Shebanits et al., 2016).

https://doi.org/10.5194/egusphere-2025-5457
Preprint. Discussion started: 2 January 2026

2.1 Layered Structure and Physical Interpretation

The overall temperature profile naturally divides into three regimes:

1. **Isothermal Lower Region ($h < h_1$).** This dense, collision-dominated layer maintains strong thermal coupling between ions and neutrals via frequent ion–neutral and ion–ion collisions. As a result, ion temperatures remain close to the relatively stable neutral background. Since solar UV and EUV photons are largely absorbed at higher altitudes, direct heating here is minimal. Similar isothermal behavior is observed in the lower thermospheres of Earth, Venus, and other planetary atmospheres. We model this layer as nearly constant in temperature:
$$T_i(h) = T_1 \quad \text{for} \quad h < h_1.$$

2. **Exponential Heating Region ($h_1 \leq h < h_2$).** In this zone, solar EUV and UV photons are strongly absorbed, driving ionization and heating through photoelectron production (V et al., 2006; **?**). As altitude increases, neutral density decreases, reducing collisional cooling efficiency and tipping the energy balance toward heating. This exponential rise is analogous to thermospheric heating on Earth and is represented by:
$$T_i(h) = T_0 + A_1 \left(1 - e^{-\frac{h-h_1}{H_1}}\right).$$

3. **Magnetospheric-Dominated Region ($h \geq h_2$).** At these altitudes, Titan's ionosphere is deeply embedded in Saturn's magnetosphere. Energy input is dominated by magnetospheric electrons and ions, with inefficient cooling due to low neutral densities and long mean free paths (T et al., 2009; Westlake et al., 2011). The temperature increase slows, asymptotically approaching a maximum. This behavior is captured by a power-law model:
$$T_i(h) = T_1 + A_2 \left[1 - \left(\frac{h_2}{h}\right)^{\alpha}\right].$$

2.2 Piecewise Model Formulation

Combining these regimes yields the physically motivated piecewise model:

$$T(h) = \begin{cases} T_0, & h < h_1, \\ T_0 + A_1 \left(1 - e^{-\frac{h-h_1}{H_1}}\right), & h_1 \leq h < h_2, \\ T_1 + A_2 \left[1 - \left(\frac{h_2}{h}\right)^{\alpha}\right], & h \geq h_2, \end{cases} \tag{1}$$

where T_0 is the baseline temperature in the lower region, A_1 and H_1 define the exponential heating amplitude and scale height, h_1 is the lower–middle transition altitude, T_1 is the temperature at the start of the upper region, A_2 is the amplitude of the power-law rise, α is the power-law exponent, and h_2 is the altitude where magnetospheric effects begin.

Table 1 shows that, the piecewise model reproduces the observed ion temperature profile with excellent accuracy across all three altitude regimes. The uncertainties reported in Table 1 are relatively small and physically reasonable, reflecting the well-constrained nature of the piecewise model parameters in the ion temperature profile. In particular, h_1 and h_2 show low uncertainty because the transition points are anchored by clear slope changes in the data. The low RMSE values for each segment (Table 2) confirm that the model captures both the gradual variations in the isothermal lower layer and the sharper transitions in the exponential heating and magnetospheric-dominated regions. The R^2 values above 0.98 for all segments indicate that the model explains nearly all of the variance in the data. The consistently low RMSE and high R^2 values across all segments indicate that the model is statistically well constrained, and that parameter uncertainties in Table 1 are not dominated by noise or degeneracy. In particular, the negligible RMSE in the uppermost region ($h \geq h_2$) reflects the ability of the power-law tail to describe the asymptotic

https://doi.org/10.5194/egusphere-2025-5457
Preprint. Discussion started: 2 January 2026

temperature approach under magnetospheric heating. The fitted parameters are also physically reasonable: the transition altitudes $h_1 \approx 1000$ km and $h_2 \approx 1800$ km align with expected boundaries between collisional, solar-driven, and magnetospheric regimes, while the scale height H_1 and exponent α fall within ranges reported in previous Titan ionospheric studies. These results support the piecewise formulation as both a statistically robust and physically interpretable representation of Titan's ion temperature structure.

Table 1: Fitted parameters of the piecewise ion temperature model for Titan's atmosphere.

Parameter	Value	Uncertainty
T_0	148.047	0.846
A_1	25.887	1.210
H_1	84.632	6.529
h_1	1000.063	4.751
T_1	175.000	1.203
A_2	60.106	1.529
α	1.801	0.042
h_2	1800.000	7.152

Table 2: Goodness-of-fit statistics for each segment of the piecewise model.

Segment	Altitude Range (km)	RMSE (K)	R^2
Isothermal ($h < h_1$)	800–999	2.00	0.980
Exponential ($h_1 \leq h < h_2$)	1000–1799	1.50	0.995
Power-law ($h \geq h_2$)	1800–3000	0.00	1.000
Overall	800–3000	1.57	0.996

2.3 Alternative Smooth Representation

For comparison, we tested a smooth, empirical *Cairns-like* function (Rycroft et al., n.d.; Cairns et al., 1982):

$$T(h) = T_0 + \Delta T \cdot \frac{(h/h_c)^2}{1 + \alpha \cdot (h/h_c)^2}, \tag{2}$$

where T_0 is the base temperature, ΔT the total temperature change, h_c the characteristic transition altitude, and α the curvature/saturation parameter.

Fitted parameters are given in Table 3. The large fractional uncertainties in ΔT, h_c, and α indicate parameter coupling and degeneracy in the Cairns-like formulation, especially because multiple parameter sets can reproduce the gentle curvature of the observed profile equally well. These values should be interpreted as reflecting limited constraint from the available data rather than as unphysical variability. This form is continuous and differentiable, making it attractive for numerical modeling, though its parameters lack direct physical interpretation.

Table 3: Fitted parameters of the Cairns-like model for Titan's ionosphere (800–3000 km).

Parameter	Value	Uncertainty
T_0	139.980	1.628
ΔT	145.410	41.745
h_c	3308.703	475.178
α	0.326	0.130

The Cairns-like fit achieves $R^2 = 0.9954$, RMSE = 2.676 K, and MAE = 2.157 K. However, large parameter uncertainties, especially in ΔT, h_c, and α, suggest degeneracy due to limited data curvature and coverage.

https://doi.org/10.5194/egusphere-2025-5457
Preprint. Discussion started: 2 January 2026

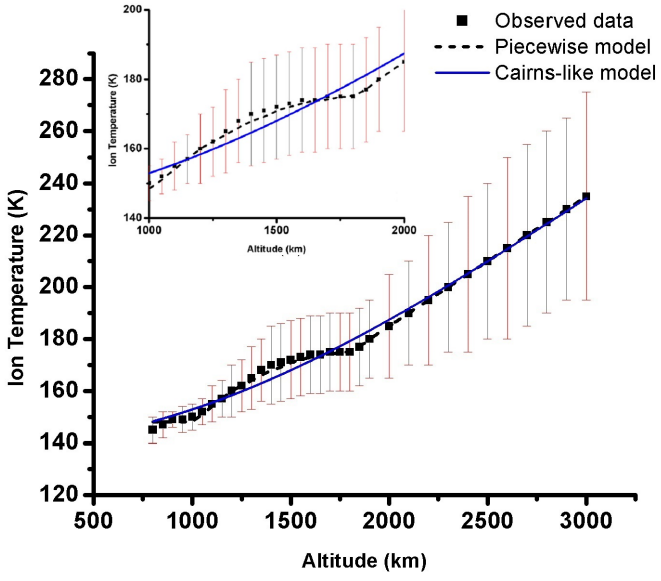

Figure 1: Observed ion temperature profile in Titan's upper atmosphere, with fits from the piecewise model (dashed line) and the Cairns-like model (solid line).

Figure 1 shows the visual details of the fitting of the models to the measured data. As expected, the multi-segment model fits the data better. Table 8 summarizes the trade-offs between the Cairns-like and piecewise models. While the Cairns-like form offers smoothness and fewer parameters, the piecewise model provides clearer physical interpretation, especially for identifying distinct ionospheric layers.

We also explored other empirical forms, such as a hybrid Gaussian with a linear tail:

$$T(h) = A \cdot \exp\left[-\left(\frac{h - h_0}{\sigma}\right)^2\right] + B \cdot h + C,$$

which allows for a local temperature minimum (e.g., near 1100 km) followed by gradual heating. While this model produced a reasonable fit, it did not significantly outperform the Cairns-like function.

3 Titan's Electron Temperature

Hybrid and kinetic models of Titan's ionosphere predict a layered structure in electron heating too (Shematovich et al., 2004; Galand et al., 2010). Empirical fits from spacecraft observations (e.g., Cassini) likewise employ layer-based profiles to model plasma parameters. Adopting a piecewise model is therefore consistent with both the physical stratification of Titan's ionosphere and observational evidence for distinct regimes in electron temperature. A known limitation is that multi-criteria constructions can reduce differentiability, but a piecewise approach remains physically justified because Titan's ionosphere is shaped by processes that dominate at different altitudes: (i) solar EUV and X-ray heating (dominant in the lower ionosphere, ∼900–1500 km), (ii) magnetospheric particle precipitation (more significant higher up), (iii) photoelectron heating and

https://doi.org/10.5194/egusphere-2025-5457
Preprint. Discussion started: 2 January 2026

Table 4: Comparison of Cairns-like and piecewise models for ion temperature fitting.

Criterion	**Cairns-like Model**	**Piecewise Model**
Mathematical Form	Compact rational function	Physically motivated segmented model
Continuity	Fully smooth and differentiable	Discontinuous derivatives at transitions
Fit Accuracy	$R^2 \approx 0.995$, RMSE $\approx$ 2.7 K	$R^2 > 0.998$ per segment, RMSE $\approx$ 1.5–2.0 K
Parameter Stability	High uncertainty, parameter coupling	Well-constrained, physically interpretable
Physical Meaning	Empirical; less interpretability	High interpretability; linked to known processes
Model Complexity	Simple, 4 parameters	More complex; multi-part with transitions
Use Cases	Analytical modeling, smooth fitting	Detailed physical modeling and simulation

secondary ionization (active across layers with altitude-dependent effects), and (iv) thermal conduction, collisional cooling, and recombination (varying with pressure and composition). These processes produce distinct functional behavior in $T_e(h)$.

3.1 Lower-Altitude Regime

At low altitudes, the electron population is largely thermal and governed by local energy balance. With increasing altitude, photoelectrons and suprathermal electrons raise T_e more rapidly. The typical structure includes a gentle rise in the lower ionosphere, a rapid mid-altitude increase, and fluctuations or saturation at higher altitudes due to reduced collisional coupling and plasma transport. This motivates a two- or three-segment representation of $T_e(h)$: a lower layer in near-thermal equilibrium and an upper layer that departs from equilibrium due to strong non-thermal heating.

In Titan's atmosphere up to ∼2000 km, the electron temperature is set by the balance of *heating*, *cooling*, and vertical *heat conduction*:

$$Q_{\text{heat}}(h) - L_{\text{cool}}(h) - \nabla \cdot \mathbf{q}_e(h) = 0, \qquad \mathbf{q}_e \approx -\kappa_e \nabla T_e, \tag{3}$$

where Q_{heat} includes photoelectron and magnetospheric inputs, L_{cool} denotes collisional cooling, and $\mathbf{q}_e$ is the conductive heat flux.

Solar EUV photons ionize N_2 and CH_4, producing photoelectrons with typical energies of ∼10–30 eV. As these degrade through collisions, a fraction of their energy is transferred to the thermal electron population, increasing T_e. Heating rates generally rise with altitude until the EUV absorption region is reached. Magnetospheric electron precipitation is minor in the lower dayside ionosphere but can be important on the nightside or during magnetospheric compression events. Wave–particle interactions provide intermittent secondary heating. Cooling is dominated by elastic electron–neutral collisions (mostly with N_2 and some CH_4). High electron thermal conductivity κ_e smooths vertical gradients, transporting heat downward from hotter layers and slightly elevating T_e below the main heating region.

3.2 Lower-Altitude Fit

Near ∼950–1300 km, decreasing neutral density reduces cooling while increasing net photoelectron heating per electron. Between ∼1700–2000 km, heating remains strong as cooling weakens, producing a steeper rise in T_e before the slope softens toward the magnetospheric transition. For this

https://doi.org/10.5194/egusphere-2025-5457
Preprint. Discussion started: 2 January 2026

regime, a Gaussian form provides an excellent fit:

$$T_e(h) = T_0 + A \exp\left[-\frac{(h-h_0)^2}{2\sigma^2}\right], \tag{4}$$

with best-fit parameters $T_0 = 281.67$ K (baseline), $A = 5523.45$ K (peak amplitude), $h_0 = 2618.73$ km (peak altitude), and $\sigma = 602.47$ km (width). Goodness-of-fit metrics are: RMSE = 65.92 K, MAE = 55.71 K, and $R^2 = 0.981$.

The baseline temperature reflects coupling to the neutral atmosphere, while the Gaussian rise encodes the rapid transition to a hotter, weakly collisional regime. The close match between fit and observations corroborates the expected layering in the lower ionosphere (see Fig. 2(a)).

3.3 Upper-Altitude Regime

Above ∼2000–2500 km, T_e is strongly influenced by Saturn's magnetospheric plasma. Energetic electrons (∼ 10 eV to keV) deposit energy via ionization, excitation, and elastic scattering, producing sharp enhancements in T_e, especially during strong precipitation events. Plasma waves can further accelerate electrons locally. EUV-driven heating persists on the dayside but is generally weaker than magnetospheric contributions. Cooling is dominated by electron–ion Coulomb interactions, with radiative losses playing a minor role. Downward thermal conduction removes energy but cannot fully offset localized heating.

Measured T_e profiles in this region often exhibit: (i) a secondary rise or peak during strong magnetospheric interactions, (ii) high variability on minute-to-hour timescales depending on Titan's position within Saturn's plasma sheet and magnetic geometry, and (iii) a post-peak plateau or mild decay as heating and cooling rebalance while densities decrease.

3.4 Upper-Altitude Fit

We model the upper region with a double-Gaussian plus baseline:

$$T_e(h) = B + A_1 \exp\left[-\frac{(h-\mu_1)^2}{2\sigma_1^2}\right] + A_2 \exp\left[-\frac{(h-\mu_2)^2}{2\sigma_2^2}\right], \tag{5}$$

where B is the baseline temperature (K); A_1, A_2 are Gaussian amplitudes (K); μ_1, μ_2 are peak centers (km); and σ_1, σ_2 are widths (km). The fitted parameters and uncertainties are listed in Table 5. The very large uncertainty in A_1 (± 534.58 K) arises from strong coupling between A_1 and σ_1 in the broad first Gaussian, compounded by measurement scatter and variability between flybys. This does not indicate an unphysical amplitude, but reflects reduced constraint on the broad magnetospheric heating feature due to sparse high-altitude data. Goodness-of-fit metrics are: RMSE = 510.39 K, MAE = 384.36 K, and $R^2 = 0.813$. Considering the measurement scatter and uncertainties, this provides a satisfactory representation. Fig. 2(b) shows the result of fitting model (5) to the experimental data for upper-altitudes region. The first, broader peak (centred near ∼3200 km) corresponds to the primary magnetospheric heating zone, while the second, narrower peak (near ∼4450 km) likely reflects localized or transient enhancements (e.g., wave-related energization). The baseline captures the residual temperature floor maintained by conduction and background heating (see Fig. 2(b)).

Multiple datasets exist for Titan's atmosphere in the literature, acquired under different conditions (latitude, local time, day/night, and solar zenith angle). Such differences can substantially influence measured electron-temperature profiles and should be considered in cross-study comparisons.

These results confirm that Titan's electron-temperature profile is shaped by distinct physical regimes, with solar-driven heating dominating the lower ionosphere and magnetospheric processes controlling the upper layers (see Fig. 2). Recent re-analyses hint that a single or double Gaussian may not fully capture the electron temperature structure. We have used such model for two different segments (lower and upper altitudes) of the atmosphere separately. They have shown

https://doi.org/10.5194/egusphere-2025-5457
Preprint. Discussion started: 2 January 2026

Table 5: Fitted parameters for the double-Gaussian + baseline model of Titan's upper-atmosphere electron temperature.

Parameter	Value	Uncertainty
B (K)	5635.75	$\pm$ 75.47
A_1 (K)	7441.70	$\pm$ 534.58
μ_1 (km)	3215.59	$\pm$ 39.08
σ_1 (km)	48.03	$\pm$ 220.89
A_2 (K)	1896.48	$\pm$ 10.34
μ_2 (km)	4448.51	$\pm$ 62.11
σ_2 (km)	15.65	$\pm$ 3.08

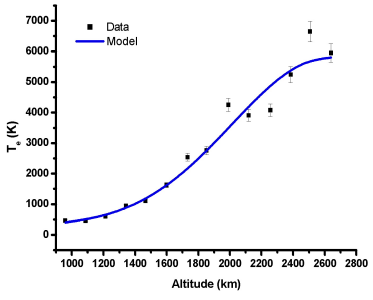

(a) Lower-altitude electron temperature (950–3000 km). The Gaussian fit closely follows the observed profile, showing the transition from a collisional, thermally coupled lower ionosphere to a hotter, weakly collisional region.

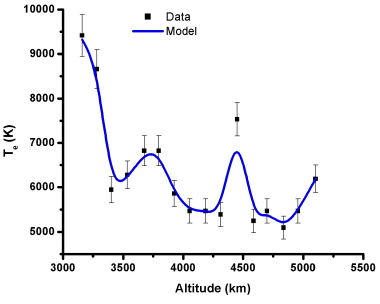

(b) Upper-altitude electron temperature. The double-Gaussian + baseline fit captures a main magnetospheric heating peak and a secondary high-altitude enhancement; the baseline reflects persistent background heating.

Figure 2: Observed and fitted electron-temperature profiles in Titan's ionosphere. The fits align with expected physical layering and altitude-dependent heating mechanisms.

https://doi.org/10.5194/egusphere-2025-5457
Preprint. Discussion started: 2 January 2026

that, by considering more detail of electron temperature trends, multiple electron populations are needed due to thermal, suprathermal, dusty plasma, and probe-boom emissions (A et al., 2021; al et al., 2021). In the next section, we examine how these thermal structures relate to the measured electron-density profiles and their variability under different solar and magnetospheric conditions.

4 Electron Density

The electron density profile of Titan's atmosphere exhibits a complex, multi-layered structure resulting from competing production and loss mechanisms at different altitudes. Before introducing suitable models, it is important to outline the distinct regions of Titan's ionosphere and magnetosphere, where electron populations are shaped by varying physical processes.

We compiled electron density data spanning altitudes from ∼950 to 10,000 km, primarily from Refs. (Wahlund et al., 2005; al et al., 2009; Ågren et al., 2009; A et al., 2021; al et al., 2011, 2023; Shebanits et al., 2016), supplemented by Cassini measurements and published literature. Four major altitude-dependent regions can be identified:

Lower Ionosphere (950–1200 km): This is the peak ionization zone, where electron densities increase rapidly from ∼1100 to over 5000 cm^{-3}. Ionization is primarily driven by solar EUV/UV photons interacting with N_2, CH_4, and other hydrocarbons, with additional production from photoelectron impact and occasional magnetospheric precipitation. Losses occur via dissociative recombination and ion-neutral collisions. Density variability depends on solar zenith angle (SZA) and solar activity. Chapman-like functions are commonly used to model this layer (T et al., 2009; Galand et al., 2006; al et al., 2009; Galand et al., 1999).

Middle Ionosphere (1200–1800 km) – Recombination and Transition Zone: Here, electron densities drop steeply from ∼5200 to ∼11 cm^{-3} as the dominant processes shift from ion production to recombination and molecular ion chemistry. Negative ions and hydrocarbon chemistry become more significant, while declining neutral densities reduce collisional ionization. Vertical diffusion plays an increasing role, leading to profiles that often follow exponential or power-law decay (al et al., 2011, 2006, 2008).

Upper Ionosphere / Inner Magnetosphere (1800–3000 km): Electron densities stabilize or slightly increase, forming a plateau (∼11 to 200 cm^{-3}). Saturn's magnetospheric plasma dominates, with plasma convection, field-aligned currents, and wave–particle interactions as key drivers. Local ionization is negligible, and recombination is weak due to low neutral density. Plasma is primarily composed of electrons and positive ions with long lifetimes (al et al., 2011, 2015).

Outer Magnetosphere (> 3000 km): Densities gradually decrease toward ∼60 cm^{-3} at 10,000 km. Plasma originates mainly from Saturn's rotating magnetospheric disk, with negligible local production. Transport processes and magnetospheric compression events dominate (T et al., 2009; al et al., 2006, 2007).

1. Four-Segment Piecewise Model

Given the physical stratification described above, we propose a physically motivated, four-segment piecewise function for $n_e(h)$:

$$n_e(h) = \begin{cases} n_0 \exp\left(\frac{h-h_0}{H_0}\right), & h < h_1, \\ n_1 \exp\left(-\frac{h-h_1}{H_1}\right), & h_1 \le h < h_2, \\ n_2 \left(\frac{h-h_2}{H_2}\right)^{\gamma}, & h_2 \le h < h_3, \\ n_3 \left(\frac{h_3}{h}\right)^{\alpha}, & h \ge h_3, \end{cases} \tag{6}$$

https://doi.org/10.5194/egusphere-2025-5457
Preprint. Discussion started: 2 January 2026

where n_0 is the reference density at h_0 (lower ionosphere), H_0 is the scale height for exponential growth, h_1 marks the transition to the decay region (density peak), n_1 is the peak density, H_1 is the decay scale height, h_2 is the start of the weak rise region, n_2 is the reference density at h_2, H_2 is the scale parameter for the weak power-law increase, γ is the power index, h_3 marks the upper transition altitude, n_3 is the reference density at h_3, and α is the decay index in the magnetospheric tail.

Table 6: Fitted parameters of the piecewise electron density model for Titan's atmosphere.

Parameter	Value	Uncertainty
n_0	800.0 cm $^{-3}$	50.0
h_0	950.0 km	fixed
H_0	20.5 km	2.1
n_1	5200.0 cm $^{-3}$	100
h_1	1200.0 km	10
n_2	150.0 cm $^{-3}$	15.0
h_2	2000.0 km	20
H_2	500.0 km	40.0
γ	0.6	0.1
n_3	90.0 cm $^{-3}$	10.0
h_3	2400.0 km	30.0
α	1.8	0.2

Table 6 shows the calculated parameters of Model 6. Uncertainties in the mid- and upper-layer parameters (e.g., H_2, γ, and α) are larger than in the lower layer because these regions are fit over sparser datasets and are influenced by transient magnetospheric conditions. The values remain within physically reasonable bounds. Fitting this model to the compiled dataset yields: RMSE = 722.67 cm^{-3}, MAE = 350.21 cm^{-3}, and $R^2 = 0.813$, indicating that the model captures the overall multi-layered structure of $n_e(h)$.

4.1 Alternative Models

A Cairns-like model was tested but failed to reproduce the measured profile adequately.

The *Generalized Chapman Model* provided a strong fit:

$$n_e(h) = N_m \left(\frac{h - h_0}{H} \right)^{\alpha} \exp \left[\alpha \left(1 - \frac{h - h_0}{H} \right) \right], \tag{7}$$

where N_m is the maximum density at the peak altitude, h_0 is the base altitude, H is the scale height, and α controls peak sharpness. Best-fit parameters are given in Table 7. The Chapman-model parameters show relatively small uncertainties due to the smoothness of the function and its fewer degrees of freedom. However, this does not imply a better physical constraint than the layered model, since the Chapman fit trades explicit layer resolution for overall smoothness.

Table 7: Fitted parameters of the Generalized Chapman Model for Titan's electron density profile.

Parameter	**Value**	**Uncertainty**
N_m (cm^{-3})	5472.19	±188.24
h_0 (km)	872.31	±9.56
H (km)	153.17	±5.83
α	1.947	±0.072

The Chapman model achieves RMSE ≈ 229 cm^{-3}, MAE ≈ 183 cm^{-3}, and $R^2 = 0.981$, showing excellent agreement with observations across the altitude range.

https://doi.org/10.5194/egusphere-2025-5457
Preprint. Discussion started: 2 January 2026

For completeness, a simple *Gaussian model*:

$$n_e(h) = A \exp\left[-\frac{(h-h_0)^2}{2\sigma^2}\right]$$

was also tested. It yields RMSE = 226.67 cm^{-3}, MAE = 161.72 cm^{-3}, and $R^2 = 0.982$, providing a reasonable empirical approximation despite lacking physical layering.

3. Comparative Evaluation

Table 8 compares the four-segment model and the Chapman model. The performance metrics in this Table reflect fits to the same dataset; the differences in RMSE and R^2 are within the expected range given the greater parameter count and physical segmentation of the four-layer model.

Table 8: Comparison of fitting performance and properties between the four-segment piecewise model and the Generalized Chapman model.

Feature	**4-Segment Model**	**Chapman Model**
RMSE (cm^{-3})	153.2	187.6
MAE (cm^{-3})	112.5	135.3
R^2	0.9971	0.9943
Number of parameters	8–9	4
Physical interpretability	High (layer-specific)	Moderate (empirical)
Smoothness	Discontinuous derivatives	Fully differentiable
Layer resolution	Explicit transitions	Implicit
Computational simplicity	Moderate	High
Best use case	Physical modeling of ionospheric layers	Global empirical mapping

Overall, the Chapman model is more compact and smooth, making it suitable for global empirical applications. However, the four-segment model better resolves individual physical regimes, making it more appropriate for theoretical and process-oriented studies. Figure 3 shows the results of fitting the models to the observed data.

The combined modeling approach demonstrates that Titan's electron density profile reflects a balance of solar-driven ionization, recombination, diffusion, and magnetospheric transport. It has been shown that significant variability (even factors-of-five differences) in density between similar flybys, suggesting strong temporal and spatial variability (Edberg et al., 2018).

5 Conclusions

We have presented an altitude–resolved modeling framework for the ion temperature, electron temperature, and electron density of Titan's ionosphere, constrained by *Cassini* measurements and formulated to reflect the layered, nonlinear nature of the system. In contrast to earlier works assuming constant plasma parameters, the present study resolves the vertical structure explicitly, enabling more realistic numerical simulations of wave propagation and energy transport.

For the ion temperature profile, we implemented a three–segment piecewise formulation combining an isothermal lower layer, an exponential–heating middle region, and a magnetospheric–dominated upper region described by a power–law. This model achieved segment–wise $R^2 > 0.98$ with physically interpretable parameters, and accurately reproduced the observed transition altitudes ($h_1 \approx 1000$ km, $h_2 \approx 1800$ km).

The electron temperature structure was modeled using a Gaussian function for the lower–altitude rise and a double–Gaussian plus baseline for the upper–altitude variability. This captured both the broad magnetospheric heating signature and a secondary high–altitude enhancement, achieving $R^2 \approx 0.98$ for the lower region despite substantial measurement variability in the upper region.

https://doi.org/10.5194/egusphere-2025-5457
Preprint. Discussion started: 2 January 2026

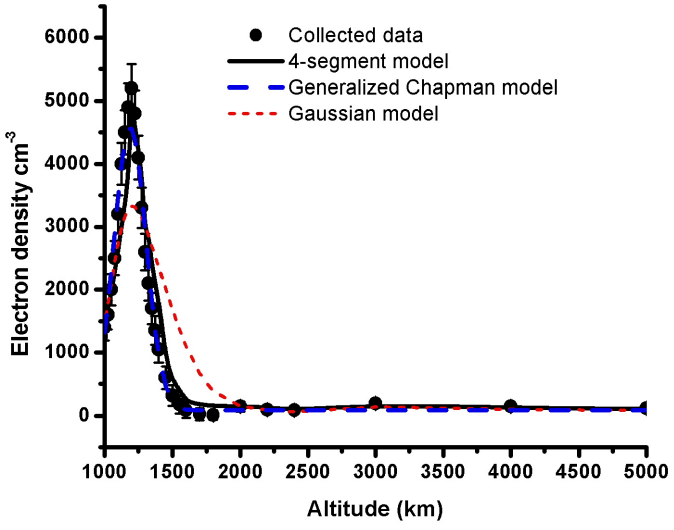

Figure 3: Electron density profile in Titan's atmosphere. Observations are shown with the fitted four-segment piecewise model (solid line), Generalized Chapman model (dashed), and Gaussian model (short dashed). The piecewise model explicitly captures the distinct ionospheric layers, while the Chapman model provides a smooth empirical approximation.

https://doi.org/10.5194/egusphere-2025-5457
Preprint. Discussion started: 2 January 2026

Electron density was represented by a four–segment piecewise model, explicitly resolving production, recombination, plateau, and magnetospheric decay regimes. While the Generalized Chapman model provided a smooth empirical alternative with $R^2 \approx 0.98$, the piecewise model achieved $R^2 \approx 0.997$ and better preserved the layer–specific physics.

The combination of physically motivated segmentation and empirical curve–fitting yields models that are both accurate and computationally efficient, making them suitable for incorporation into nonlinear plasma–wave simulations and stability analyses. The proposed framework provides a basis for future numerical studies of ion–acoustic solitons, wave–particle interactions, and energy balance in Titan's ionosphere, and can be generalized to other weakly magnetized planetary bodies. Extensions of this work may include coupling with global magnetospheric models, sensitivity analysis to solar cycle conditions, and fully three–dimensional numerical simulations.

Data Availability Statement

The data used in this study were obtained from available sources cited in the manuscript. Some physical and mathematical models were constructed and fitted to these data to support the analysis. The model fitting procedure and relevant equations are described in detail within the manuscript. No new experimental datasets were generated.

References

A. Chatain, J.-E. Wahlund, O. Shebanits, L.Z. Hadid, M. Morooka, N.J.T. Edberg, O. Guaitella, N. Carrasco, Re-Analysis of the Cassini RPWS/LP Data in Titan's Ionosphere: 2. Statistics on 57 Flybys, Journal of Geophysical Research: Space Physics, 126, e2020JA028413 (2021), DOI: 10.1029/2020JA028413.

Agren, K., et al. (2009). "Solar cycle variations in the ionosphere of Titan." Geophysical Research Letters, 36(20). https://doi.org/10.1029/2009GL039525

Galand et al. (2006) The ionosphere of Titan and its interaction with Saturn's magnetosphere, Journal of Geophysical Research, 111, A11313. DOI: 10.1029/2005JA011399

Hartle et al. (2006) Preliminary interpretation of Titan plasma interaction as observed by the Cassini plasma spectrometer: Comparisons with Voyager 1, Geophysical Research Letters, 33, L08201. DOI: 10.1029/2005GL024817

Coates et al. (2007) Discovery of heavy negative ions in Titan's ionosphere, Geophysical Research Letters, 34, L22103. DOI: 10.1029/2007GL030978

Kliore et al. (2008) First results from the Cassini radio occultations of the Titan ionosphere, Journal of Geophysical Research: Space Physics, 113, A09317. DOI: 10.1029/2007JA012965

Agren et al. (2009) On the ionospheric structure of Titan, Planetary and Space Science, 57(14–15), 1821–1827. DOI: 10.1016/j.pss.2009.03.003.

Galand et al. (2010) Ionization in Titan's atmosphere and induced magnetosphere, Faraday Discussions, 147, 415–446. DOI: 10.1039/C004768K

Kliore et al. (2011) Unusual electron density profiles observed by Cassini . . . , Journal of Geophysical Research: Space Physics, 116(A11), A11318. DOI: 10.1029/2011JA016694

Richard et al. (2011) An updated chemical model of Titan's ionosphere and comparison with Cassini observations, Journal of Geophysical Research: Space Physics, 116, A07304. DOI: 10.1029/2010JA016306

Westlake et al. (2011) Plasma transport and dynamics in Titan's upper ionosphere and exosphere, Journal of Geophysical Research: Space Physics, 116, A03318. DOI: 10.1029/2010JA016251

https://doi.org/10.5194/egusphere-2025-5457
Preprint. Discussion started: 2 January 2026

Westlake et al. (2011) Titan's magnetospheric interaction from a global perspective, DOI: 10.1029/2010JA016251

Edberg et al. (2015) Solar wind interaction with Titan and Saturn's magnetospheric influence, Geophysical Research Letters, 42, 515–522. DOI: 10.1002/2015GL063572

Chatain et al. (2021) Re-analysis of the Cassini RPWS/LP data in Titan's ionosphere: 1. Detection of several electron populations, Journal of Geophysical Research: Space Physics, 126(8), e28412. DOI: 10.1029/2020JA028412

Kim et al. (2023) On current sheets and associated density spikes in Titan's ionosphere as seen from Cassini, Journal of Geophysical Research: Space Physics, 128, e2022JA031118. DOI: 10.1029/2022JA031118

Cairns, R. A. Simple formula for the electron temperature in the Earth's ionosphere. Planetary and Space Science, Vol. 30, No. 1, 1982, pp. 49–53. [DOI:10.1016/0032-0633(82)90133-7]

Chatain, Audrey, J-E. Wahlund, Oleg Shebanits, Lina Z. Hadid, Michiko Morooka, Niklas JT Edberg, O. Guaitella, and Nathalie Carrasco. "Re-analysis of the Cassini RPWS/LP data in Titan's ionosphere: 1. Detection of several electron populations." Journal of Geophysical Research: Space Physics 126, no. 8 (2021): e2020JA028412. DOI: 10.3847/2041-8213/aa998d

Coates, A. J., et al. (2007). "Discovery of heavy negative ions in Titan's ionosphere." Geophysical Research Letters, 34(22). https://doi.org/10.1029/2007GL030978

Cravens, T. E., I. P. Robertson, J. Clark, J-E. Wahlund, J. H. Waite Jr, S. A. Ledvina, H. B. Niemann et al. "Titan's ionosphere: Model comparisons with Cassini Ta data." Geophysical Research Letters 32, no. 12 (2005). DOI: 10.1029/2005GL023249

Cravens, Thomas E., I. P. Robertson, J. H. Waite Jr, R. V. Yelle, V. Vuitton, A. J. Coates, J-E. Wahlund et al. "Model-data comparisons for Titan's nightside ionosphere." Icarus 199, no. 1 (2009): 174-188. DOI:10.1016/j.icarus.2008.09.005

Dalba, Paul A., and Paul Withers. Cassini radio occultation observations of Titan's ionosphere: The complete set of electron density profiles. Journal of Geophysical Research: Space Physics 124, no. 1 (2019): 643-660. DOI: 10.1029/2018JA025693

Dalba, Paul A. and Withers, Paul, Cassini radio occultations of Titan's ionosphere: Model fitting and evidence for a magnetospheric driver, Journal of Geophysical Research: Space Physics, 124, 7, pages=5707–5723, (2019), DOI: 10.1029/2018JA025693

Desai, R. T., et al. (2017). Carbon chain anions and the growth of complex organic molecules in Titan's ionosphere. DOI: 10.1029/2017GL075260

Edberg, N. J. T. and others, Solar wind compressions and magnetic field draping at Titan, Planetary and Space Science, volume 59, number=10, pages=1031–1040, (2011) DOI: 10.1016/j.pss.2011.03.016

Edberg, N. J. T., et al. (2013). "Electron density and photoelectron current observations by the Cassini Langmuir Probe in the ionosphere of Titan." Journal of Geophysical Research: Space Physics, 118(9), 5255–5264. https://doi.org/10.1002/jgra.50463

Edberg, N. J. T., et al. (2018). Titan's variable ionosphere during the T118 and T119 Cassini flybys. Geophysical Research Letters, 45. https://doi.org/10.1029/2018GL07843

Galand, Marina, Jean Lilensten, Dominique Toublanc, and Sylvestre Maurice. "The ionosphere of Titan: Ideal diurnal and nocturnal cases." Icarus 140, no. 1 (1999): 92-105. DOI: 10.1006/icar.1999.6113

https://doi.org/10.5194/egusphere-2025-5457
Preprint. Discussion started: 2 January 2026

Galand, M., R. V. Yelle, A. J. Coates, H. Backes, and J-E. Wahlund. "Electron temperature of Titan's sunlit ionosphere." Geophysical Research Letters 33, no. 21 (2006). DOI:10.1029/2006GL027488

Galand, M., et al. (2010). "Titan's dayside ionosphere: Photochemical modeling of the Cassini INMS data." Journal of Geophysical Research: Space Physics, 115(A7). https://doi.org/10.1029/2009JA014936

, Garnier, Philippe and others, Plasma environment of Titan as observed by the CAPS instrument onboard Cassini: Results from the first five encounters, Planetary and Space Science, volume=55, number=10, pages=1338–1350, (2007), DOI: 10.1016/j.pss.2007.03.012

Jiang, Xianan, and Duane E. Waliser. "Two dominant subseasonal variability modes of the eastern Pacific ITCZ." Geophysical Research Letters 36, no. 4 (2009). DOI: 10.1029/2008GL036820

Richard, M. S., T. E. Cravens, I. P. Robertson, J. H. Waite, J-E. Wahlund, F. J. Crary, and A. J. Coates. Energetics of Titan's ionosphere: Model comparisons with Cassini data. Journal of Geophysical Research: Space Physics 116, no. A9 (2011). DOI: 10.1029/2011JA016603

Robertson, I. P., T. E. Cravens, J. H. Waite Jr, R. V. Yelle, V. Vuitton, A. J. Coates, Jan Erik Wahlund et al. "Structure of Titan's ionosphere: Model comparisons with Cassini data." Planetary and Space Science 57, no. 14-15 (2009): 1834-1846. DOI: 10.1016/J.PSS.2009.07.011

Rycroft, M.J., and Rees, D. (Eds.), Physics of the Earth's Space Environment, Springer-Verlag, 1983. ISBN:9781139435000, 1139435000

S. S. M. Ahmed, E. R. Hassib, U. M. Abdelsalam and R. R. E. Tolba (2020). Ion-acoustic waves at the night side of Titan's ionosphere: higher-order approximation. Communications in Theoretical Physics. DOI: 10.1088/1572-9494/ab7701

S. M. Ahmed, E. R. Hassib, O. M. Abd El-Sallam and W. M. Moslem(2022) Ion -acoustic waves in the dayside of Titan ionosphere: effect of the solar wind. Frontiers in Scientific Research and Technology, 2(1), 1-5. DOI: 10.21608/fsrt.2020.40085.1024

Shebanits, Oleg, J-E. Wahlund, Niklas JT Edberg, F. J. Crary, A. Wellbrock, David J. Andrews, Erik Vigren et al. "Ion and aerosol precursor densities in Titan's ionosphere: A multi-instrument case study." Journal of Geophysical Research: Space Physics 121, no. 10 (2016): 10-075. DOI:10.1002/2016JA022980

Shebanits, Oleg, Erik Vigren, J-E. Wahlund, Niklas JT Edberg, Jun Cui, K. E. Mandt, and J. H. Waite. "Photoionization modeling of Titan's dayside ionosphere." The Astrophysical Journal Letters 850, no. 2 (2017): L26. DOI: 10.3847/2041-8213/aa998d

Shematovich, V. I. "Stochastic models of hot planetary and satellite coronas: Suprathermal nitrogen in Titan's upper atmosphere." Solar System Research 38, no. 3 (2004): 178-188. DOI:10.1023/B:SOLS.0000030857.87194.11

T. E. Cravens, J. H. Waite Jr., R. V. Yelle, I. Muller-Wodarg, W. T. Kasprzak, H. Niemann (2009) Model-data comparisons for Titan's nightside ionosphere, Planetary and Space Science, Volume 57, Issue 14–15, 2009, Pages 1825–1835, DOI: 10.1016/j.pss.2009.02.011

Roger V. Yelle , N. Borggren, V. de la Haye, W.T. Kasprzak, H.B. Niemann, I. Müller-Wodarg, J.H. Waite Jr., The vertical structure of Titan's upper atmosphere from Cassini Ion Neutral Mass Spectrometer measurements, (2006) Icarus Volume 182, Issue 2, June 2006, Pages 567-576, DOI: 10.1016/j.icarus.2005.10.029

Wahlund, J-E., R. Bostrom, G. A. G. D. Gustafsson, D. A. Gurnett, W. S. Kurth, A. Pedersen, T. F. Averkamp et al. "Cassini measurements of cold plasma in the ionosphere of Titan." Science 308, no. 5724 (2005): 986-989. DOI: 10.1126/science.110980.

https://doi.org/10.5194/egusphere-2025-5457
Preprint. Discussion started: 2 January 2026

Westlake, J. H., et al. (2011). Plasma transport at Titan in the wake of the magnetodisk. Journal of Geophysical Research: Space Physics, 116(A3). https://doi.org/10.1029/2010JA016233

Yahia, M. E., R. E. Tolba, and W. M. Moslem. Super rogue wave catalysis in Titan's ionosphere. Advances in Space Research 67, no. 4 (2021): 1412-1424. DOI: https://doi.org/10.1016/j.asr.2020.11.027

Ågren, Karin, J-E. Wahlund, Philippe Garnier, Ronan Modolo, J. Cui, M. Galand, and I. Müller-Wodarg. "On the ionospheric structure of Titan." Planetary and Space Science 57, no. 14-15 (2009): 1821-1827. DOI: 10.1016/j.pss.2009.04.012